Journal of Molecular Catalysis A: Chemical 335 (2011) 129–135

Contents lists available at ScienceDirect

Journal of Molecular Catalysis A: Chemical

journal homepage: www.elsevier.com/locate/molcata

Aqueous-phase reforming of ethylene glycol on Co/ZnO catalysts prepared by the coprecipitation method

Xianwen Chu, Jun Liu, Bo Sun, Rui Dai, Yan Pei*, Minghua Qiao**, Kangnian Fan

Department of Chemistry and Shanghai Key Laboratory of Molecular Catalysis and Innovative Materials, Fudan University, No. 220 Handan Road, Shanghai 200433, PR China

ARTICLE INFO

Article history:
Received 15 September 2010
Received in revised form
19 November 2010
Accepted 22 November 2010
Available online 2 December 2010

Keywords:
Co/ZnO
Coprecipitation
Ethylene glycol
Aqueous-phase reforming
Hydrogen

ABSTRACT

Co/ZnO catalysts with different Co/Zn ratios have been prepared by the coprecipitation method. It is revealed that below the nominal Co/Zn molar ratio of 2, the calcined Co/ZnO samples were constituted by ZnO and $ZnCo_2O_4$ spinel. At the nominal Co/Zn ratio of 2, a small amount of Co_3O_4 spinel emerged. After reduction, the catalysts were composed of fcc Co and ZnO. In aqueous-phase reforming (APR) of ethylene glycol, it is found that the intrinsic activity and selectivity to H_2 increase with the increment of the ZnO content. H_2 selectivities over the Co/ZnO catalysts ranged from 52% to 89%, which are substantially higher than that of the Raney Ni catalyst at similar conversion. Moreover, the Co/ZnO catalysts produced much less CO in the product gas. With the aid of literature works as well as additional experiments on APR of acetic acid, methanol, and ethanol, the reaction pathways of ethylene glycol in the presence of water on the Co/ZnO catalysts were discussed.

1. Introduction

Approximately 80% of the present world energy demand comes from fossil fuels [1], which are exhaustible and cause serious environmental problems. Recently, Dumesic and coworkers demonstrated the new process of aqueous-phase reforming (APR) of biomass-derived polyols such as ethylene glycol, glycerol, and sorbitol to H_2 and hydrocarbons [2–4]. The APR process is operated at temperatures near 500 K, at which the water–gas shift (WGS) reaction is thermodynamically favored, making it possible to generate H_2 and hydrocarbons in a single reactor with trace amount of CO [5]. This process is energy-efficient and green-house gas-neutral, thus opening a new opportunity for the utilization of readily available renewable biomass.

Catalysts that have been studied in the APR of ethylene glycol include Pt-based catalysts [2,6–13], SiO_2-supported Ni, Pd, Ru, Rh, and Ir catalysts [6], Sn-modified Raney Ni [3,8,14,15], Ni/Al_2O_3 catalysts [8,14], rapidly quenched skeletal Ni [16] and NiMo catalysts [17], and non-pyrophoric Ni catalyst derived from traditional $Ni_{50}Al_{50}$ alloy [18]. However, the APR performance of Co-based catalyst has not been explored as far as we are aware of. It is acknowledged that Co exhibits appreciable activities for C–C bond scission, WGS, and Fischer–Tropsch synthesis (FTS) among VIIIB metals [6,19], so the Co-based catalyst is anticipated to be promising for the APR process.

It has been shown that the Co-based catalysts are efficient in steam reforming (SR) of ethanol [20]. Homs and coworkers have prepared Co catalysts by impregnating $Co_2(CO)_8$ on a series of supports, and found that the ZnO-supported Co catalyst exhibited the best catalytic performance in SR of ethanol [21]. Motivated by their work, we prepared Co/ZnO catalysts with different Co/Zn ratios by the coprecipitation method using less hazardous cobalt nitrate. Their catalytic behaviors in APR of ethylene glycol were investigated and correlated with the characterization results. The reaction pathways of ethylene glycol on the Co/ZnO catalysts in the presence of water were discussed with the aid of additional experiments on APR of acetic acid, methanol, and ethanol.

2. Experimental

2.1. Catalyst preparation

The Co/ZnO catalysts with four different Co/Zn molar ratios were prepared by the coprecipitation method. An aqueous solution fixed at 0.4 M containing a mixture of $Zn(NO_3)_2$ and $Co(NO_3)_2$ was added drop by drop to an aqueous solution of Na_2CO_3 (0.4 M) as the precipitant at 333 K under stirring. After being aged at 333 K for 2 h, the solid was filtered, washed with deionized water to neutrality, dried at 373 K overnight, and then calcined at 723 K for 4 h at a heating rate of 10 K min^{-1} in static air. The catalysts were obtained by reduction under 5 vol.% H_2/Ar at 723 K for 2 h at a heating rate of

* Corresponding author. Tel.: +86 21 55664679; fax: +86 21 6562978.
** Corresponding author. Tel.: +86 21 55664679; fax: +86 21 6562978.
E-mail addresses: peiyan@fudan.edu.cn (Y. Pei), mhqiao@fudan.edu.cn (M. Qiao).

1381-1169/$ – see front matter © 2010 Elsevier B.V. All rights reserved.
doi:10.1016/j.molcata.2010.11.024

Table 1
Physicochemical properties of the Co and Co/ZnO samples before and after reduction.

Sample	Co/Zn (molar ratio)		S_{BET} ($m^2\ g^{-1}$)		$d_{ZnCo_2O_4}$ (nm)[a]	d_{Co}[a] (nm)	d_{ZnO}[a] (nm)		S_H[b] ($m^2\ g^{-1}$)
	Nominal	Exp.	Cal.	Red.			Cal.	Red.	
Co/ZnO-13	0.33	0.5	41	12	12	20	14	23	1.1
Co/ZnO-12	0.5	0.8	44	11	13	24	13	28	1.3
Co/ZnO-11	1.0	1.3	45	11	13	27	10	27	1.8
Co/ZnO-21	2.0	2.2	47	9	12	28	/	27	2.3
Co_3O_4	/	/	42	2	20 (Co_3O_4)	71	/	/	0.2

[a] Crystallite size determined by XRD.
[b] Active surface area determined by H_2 chemisorption.

1 K min^{-1}. The nominal Co/Zn molar ratios were 1/3, 1/2, 1/1, and 2/1 for catalysts labeled Co/ZnO-13, Co/ZnO-12, Co/ZnO-11, and Co/ZnO-21, respectively. Co_3O_4 was prepared in a way similar to that of the calcined Co/ZnO samples in the absence of $Zn(NO_3)_2$. We have also prepared the Co/ZnO-13 catalyst by the impregnation method (Co/ZnO-13-imp). However, it is identified that the catalytic performance in APR of ethylene glycol on the Co/ZnO-13-imp catalyst was much inferior to that on the Co/ZnO-13 catalyst prepared by the coprecipitation method.

2.2. Catalyst characterization

The bulk composition was determined by inductively coupled plasma-atomic emission spectroscopy (ICP-AES; Thermo Elemental IRIS Intrepid). The BET surface area was measured on a Micromeritics TriStar3000 adsorption apparatus by N_2 physisorption at 77 K. Prior to the measurement, the sample in the glass adsorption tube was degassed at 423 K under a N_2 flow for 2 h.

X-ray diffraction patterns (XRD) were acquired on a Bruker D8 Advance X-ray diffractometer using Ni-filtered Cu Kα radiation (1.5418 Å) with a scanning angle (2θ) of 10–90°. The voltage was 40 kV, and the current was 40 mA. The Scherrer equation was used to estimate the crystallite size. Temperature-programmed reduction (TPR) profiles were collected on a home-made apparatus with the 5 vol.% H_2/Ar flow rate of 40 ml min^{-1} and the heating rate of 10 K min^{-1}. The amount of H_2 consumed was quantified with a thermal conductivity detector (TCD).

H_2 chemisorption was carried out on a home-made apparatus equipped with a TCD detector. A catalyst sample of ca. 300 mg was reduced at 723 K for 2 h in 5 vol.% H_2/Ar. After reduction, the temperature was kept at 723 K for 2 h and then cooled to room temperature in an Ar flow. The chemisorption was carried out at 423 K, and the metal surface area (S_H) of the catalyst was calculated based on the assumption of a H:Co stoichiometry of 1:1 according to Reuel and Bartholomew [22].

The surface morphology was observed by transmission electron microscopy (TEM; JEOL JEM2011). X-ray photoelectron spectrum (XPS; Perkin Elmer PHI5000C) was recorded using Mg Kα radiation as the excitation source (1253.6 eV). The sample, pressed into a self-supported disc, was mounted on the sample plate and degassed in the pretreatment chamber in vacuo at room temperature for 4 h. The sample was then transferred to the analyzing chamber with a background pressure better than 2×10^{-9} Torr. All binding energy (BE) values were referenced to the C 1 s peak of contaminant carbon at 284.6 eV with an uncertainty of ±0.2 eV.

2.3. Activity test and product analysis

A reactor system similar to that of Shabaker et al. [7] was used for APR of ethylene glycol. An aqueous solution containing 5 wt% of ethylene glycol was fed to the reactor in an up-flow configuration. The reforming was operated at a temperature of 498 K, system pressure of 2.58 MPa, and WHSV ((weight flow rate of the feed solution) × (weight fraction of ethylene glycol in the feed)/(weight of the catalyst)) of 0.59 h^{-1} if not specified. Argon was used to regulate the system pressure. The reaction course was monitored by sampling the gas and liquid products at intervals, followed by gas chromatographic analysis. For the gas effluent, H_2, CO, CH_4, and CO_2 were separated by a 5 Å molecular sieve-packed column, and examined by TCD. CH_4, C_2H_4, C_2H_6, C_3H_6, C_3H_8, C_4H_8, and C_4H_{10} were separated by a Porapak R packed column, and examined by a flame ionization detector (FID). The liquid effluent was separated by a CP-Wax 52 CB capillary column (30 m × 0.25 mm × 0.25 μm), and examined by FID [16]. The selectivities to H_2 and hydrocarbons were calculated based on independent hydrogen and carbon balances, respectively [14]. Steady-state product compositions were achieved after 6 h on stream.

3. Results and discussion

3.1. Physicochemical properties

Table 1 lists the bulk compositions and BET surface areas of the Co/ZnO samples. It is found that the experimental Co/Zn molar ratios always exceed the nominal values, suggesting that zinc cations are more reluctant to precipitate than cobalt cations under the present preparation conditions. With the increment of the Co/Zn ratio, the experimental ratios approach the nominal values. For the calcined Co/ZnO samples, the BET surface area increases slightly from 41 to 47 $m^2\ g^{-1}$ with the increment of the nominal Co/Zn ratio from 1/3 to 2/1. After reduction, the BET surface areas of all the Co/ZnO catalysts are decreased to about 10 $m^2\ g^{-1}$.

The XRD patterns of the calcined Co/ZnO samples are shown in Fig. 1a. For the Co/ZnO-13 sample with the lowest Co/Zn ratio, the diffraction peaks can be assigned to a combination of ZnO (JCPDS 36-1451) and $ZnCo_2O_4$ (JCPDS 23-1390) or Co_3O_4 (JCPDS 42-1467). It is noted that the last two spinel phases are indistinguishable by XRD, because their standard diffractograms are similar. However, one can find in Fig. 1a that with the increment of the Co/Zn ratio, the diffraction peaks of ZnO are attenuated, and nearly disappear for the Co/ZnO-21 sample with the nominal Co/Zn molar ratio of 2, a stoichiometry identical to that in $ZnCo_2O_4$. This phenomenon strongly suggests the formation of $ZnCo_2O_4$ rather than Co_3O_4 in the calcined Co/ZnO samples. For the Co/ZnO-21 sample, Table 1 shows that the experimental Co/Zn molar ratio is 2.2, implying that in this sample about 10% of Co is in the form of Co_3O_4. For comparison, Homs and coworkers identified exclusively Co_3O_4 on their calcined Co/ZnO sample prepared by the impregnation method [23], suggesting that the coprecipitation method results in a stronger interaction between the oxides of cobalt and zinc.

After reduction, Fig. 1b shows that $ZnCo_2O_4$ as well as Co_3O_4 for the Co/ZnO-21 sample originally in the calcined Co/ZnO samples are diminished. Instead, new features at 2θ of 44.3, 51.5, and 75.9° ascribable to fcc Co (JCPDS 15-0806) emerge. The diffraction peaks of ZnO, which are not available on the calcined Co/ZnO-21 sample, are identified after reduction, signifying the decomposition of

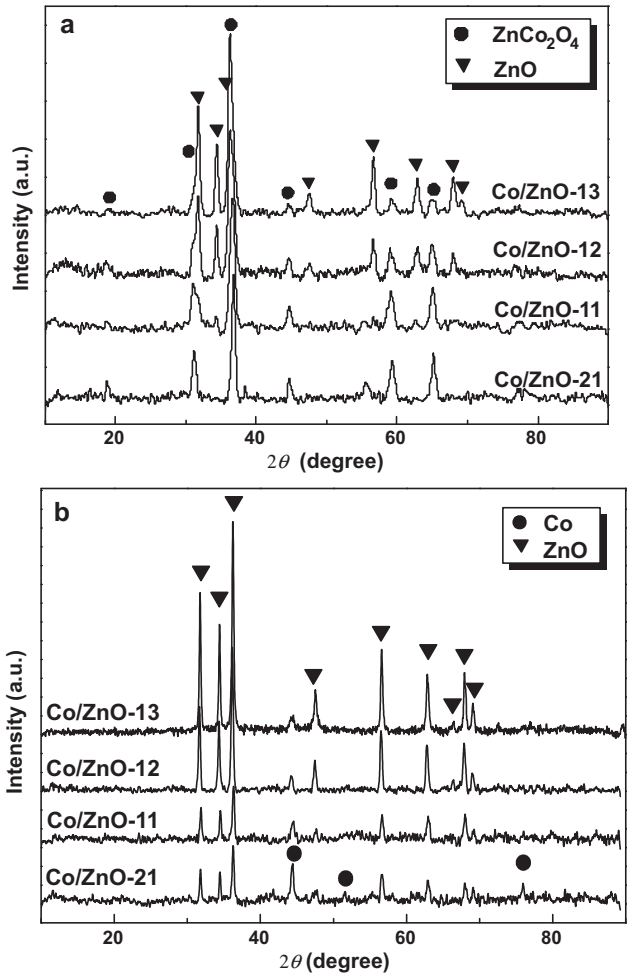

Fig. 1. XRD patterns of the Co/ZnO samples (a) before and (b) after reduction.

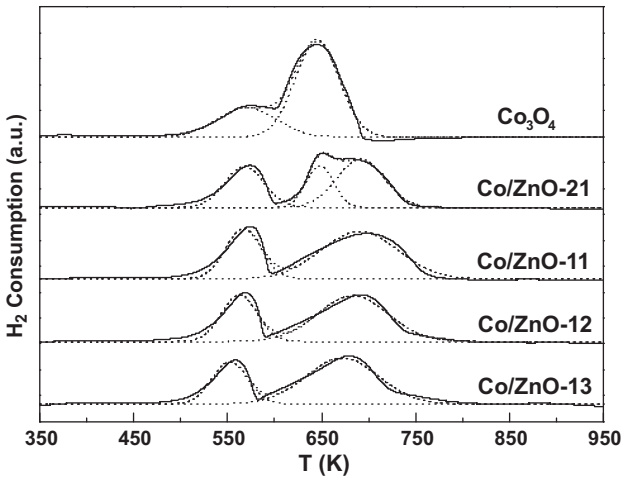

Fig. 2. H_2-TPR profiles of Co_3O_4 and the Co/ZnO samples.

$ZnCo_2O_4$ to ZnO and Co. Moreover, the diffraction peaks of ZnO are very sharp for the reduced catalysts. Based on X-ray line broadening, the crystallite sizes of ZnO, $ZnCo_2O_4$, and metallic Co in the calcined and reduced Co/ZnO samples are calculated. Table 1 shows that the crystallite sizes of ZnO and metallic Co in the reduced catalysts are about twice as those of ZnO and $ZnCo_2O_4$ in the calcined counterparts, which can be an important reason for the decreased BET surface areas after reduction.

Fig. 2 shows the H_2-TPR profiles of the Co/ZnO samples. The reduction degree of the Co/ZnO-13, Co/ZnO-12, Co/ZnO-11, and Co/ZnO-21 catalysts are 86%, 91%, 94%, and 95%, respectively. The TPR profile of a Co_3O_4 sample is also presented in the figure for comparison. Co_3O_4 shows two distinct H_2 consumption peaks centered at 575 and 644 K, with the intensity ratio between the low- and high-temperature peaks being ca. 1/3, which corresponds exactly to a two-step reduction mechanism of Co_3O_4 ($Co_3O_4 + H_2 \rightarrow 3CoO + H_2O$, $3CoO + 3H_2 \rightarrow 3Co + 3H_2O$) [24]. On the other hand, the TPR profiles of the calcined Co/ZnO-13, Co/ZnO-12, and Co/ZnO-11 samples are similar to each other. These samples also give two H_2 consumption peaks, but the peak maxima (573 and 700 K) deviate noticeably from those of Co_3O_4. Moreover, the intensity ratio of the peak area between the low- and high-temperature peaks for these samples is ca. 1/1.99, which conforms to the stoichoimetry of the two-step reduction mechanism of $ZnCo_2O_4$ ($ZnCo_2O_4 + H_2 \rightarrow 2CoO + ZnO + H_2O$, $2CoO + 2H_2 \rightarrow 2Co + 2H_2O$) [25–27].

For the calcined Co/ZnO-21 sample, although its TPR profile resembles more the profiles of other Co/ZnO samples, it is evident that there is an additional shoulder peak at 647 K superposing on the high-temperature peak. This shoulder peak appears at a temperature close to that of the high-temperature peak of Co_3O_4, suggesting their similar origin. We also integrated the areas of the low-temperature peak and the high-temperature peak including the shoulder peak, and obtained a ratio of 1/2.22. This ratio is much larger than that of Co_3O_4, while slightly smaller than that of $ZnCo_2O_4$, signifying again that the major phase in the calcined Co/ZnO-21 sample is $ZnCo_2O_4$.

The TEM images of the reduced Co/ZnO catalysts are presented in Fig. 3. The dark metallic Co nanoparticles are dispersed on the platelet-like ZnO. The average particle size of metallic Co measured in the TEM images increases from about 25 to 50 nm with the nominal Co/Zn molar ratio from 1/3 to 2/1, while the particle size of ZnO is in the range of 45–80 nm for all the catalysts. The particle sizes of Co and ZnO observed in Fig. 3 are much larger than the crystallite sizes derived from XRD, suggesting their polycrystalline nature.

Fig. 4a presents the HRTEM image of the calcined Co/ZnO-13 sample. The lattice fringes in direct space corresponding to the (1 1 1) plane of $ZnCo_2O_4$ of 4.66 Å and the (1 0 1) plane of ZnO of 2.48 Å are readily visible. Fig. 4b shows the HRTEM image of the reduced Co/ZnO-13 catalyst. The particle labeled 'A' on top of the ZnO platelet displays a complex high-resolution image. The Fourier transform image of this area affords spots corresponding to the Co(1 1 1) diffraction at 2.04 Å and the ZnO(1 0 1) diffraction at 2.48 Å, which are consistent with the assignments based on XRD. The highly defective structure of area 'A' may be an indication of the out-growth of metallic Co from the bulk of the $ZnCo_2O_4$ spinel during the reduction process.

Fig. 5 shows the Co 2p spectra of the calcined and the reduced Co/ZnO samples. For the calcined samples (Fig. 5a), the Co $2p_{3/2}$ BE is 780.4 eV, and the BE difference between the $2p_{1/2}$ and $2p_{3/2}$ levels is 15.0 eV, which can be ascribed either to $ZnCo_2O_4$ or to Co_3O_4 which are not distinguishable if only based on these two parameters [28,29]. However, compared with the standard Co 2p spectra of $ZnCo_2O_4$ and Co_3O_4 reported by Zsoldos and Guczi [28], the presence of a weak satellite peak at ca. 9 eV higher than the Co $2p_{3/2}$ peak observed in Fig. 5a supports the formation of predominantly $ZnCo_2O_4$.

After reduction, Fig. 5b shows that there are two Co $2p_{3/2}$ peaks with BEs of 778.0 and 780.2 eV, respectively. The former is readily assignable to metallic Co [30], while the latter, combining with the strong satellite peak at ca. 6 eV higher BE, is assigned to CoO [31].

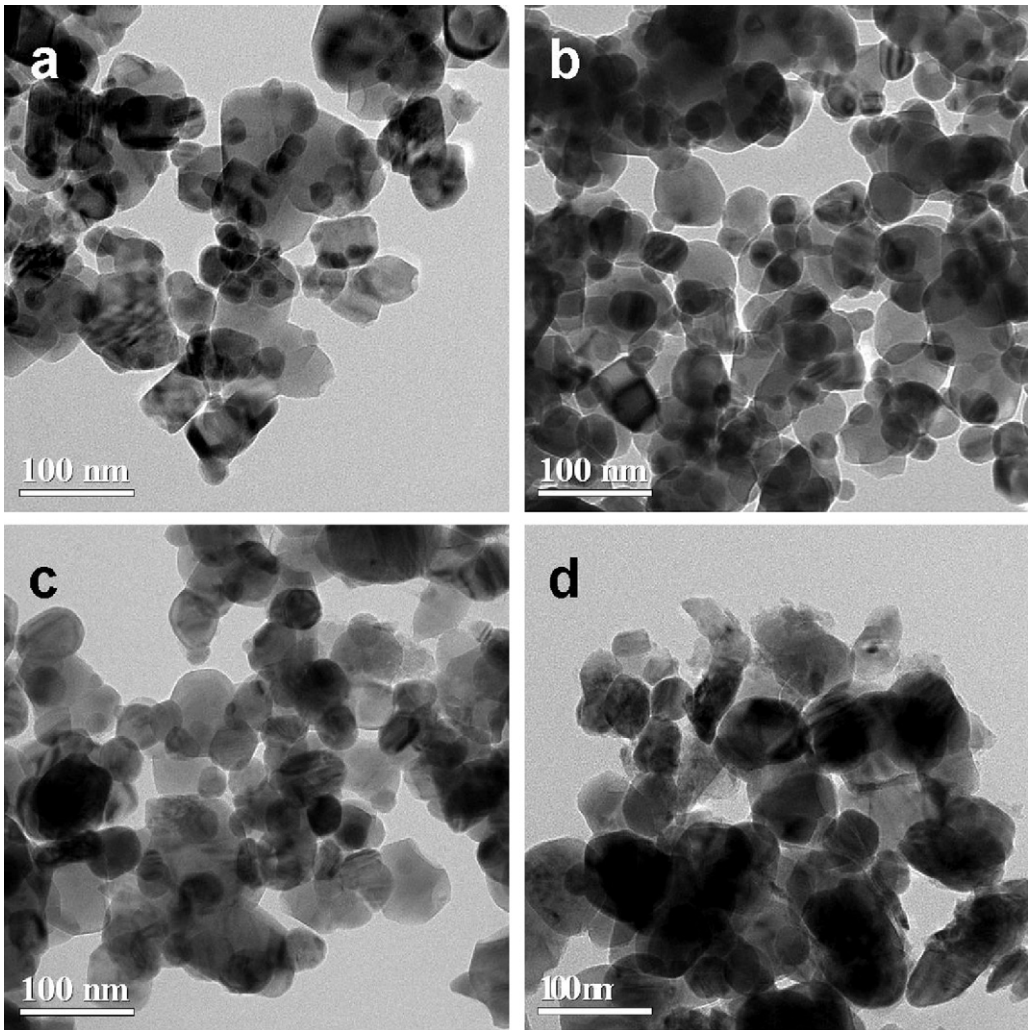

Fig. 3. TEM images of Co/ZnO catalysts after reduction. (a) Co/ZnO-13, (b) Co/ZnO-12, and (c) Co/ZnO-11, and (d) Co/ZnO-21.

It is observed that the proportion of metallic Co increases with the increment of the Co/Zn ratio, which is consistent with the ascending active surface area (S_H, Table 1) and reduction degree with the increment of the Co/Zn ratio.

3.2. APR performance

Table 2 compiles the selectivities to H_2 and hydrocarbons and kinetic data for APR of ethylene glycol over the Co/ZnO catalysts

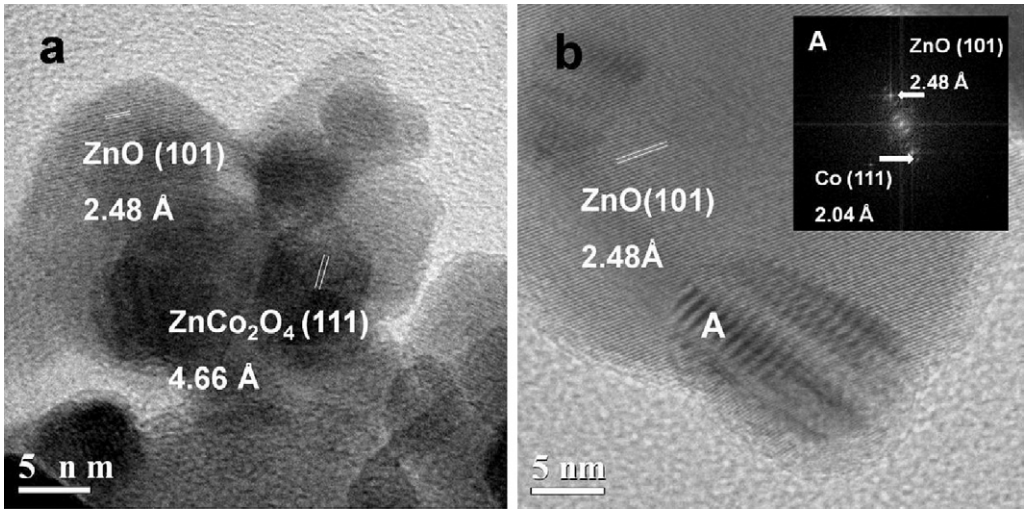

Fig. 4. HRTEM images of the Co/ZnO-13 sample (a) before and (b) after reduction. The inset corresponds to the Fourier-transformed image of area marked as 'A'.

Table 2
Kinetic results over the Co/ZnO catalysts in APR of 5 wt% ethylene glycol at 498 K, 2.58 MPa, WHSV of 0.59 h^{-1}, and after 8 h on stream.

Catalyst	Co/ZnO-13	Co/ZnO-12	Co/ZnO-11	Co/ZnO-21
Conversion of EG to gas (%)	5.2	6.2	7.5	8.6
Conversion of EG to liquid (%)	1.6	1.5	1.4	1.4
H_2 selectivity[a] (%)	89	77	58	52
Hydrocarbon selectivity[b] (%)	29	36	41	46
TOF of gas products (h^{-1})				
H_2	101.4	76.0	40.6	27.9
CO	n.d.[c]	n.d.	n.d.	n.d.
CO_2	32.2	25.6	16.4	11.5
CH_4	8.1	9.2	7.8	6.7
C_2H_4	0.07	0.06	0.04	0.03
C_2H_6	0.69	0.68	0.52	0.44
C_3H_6	0.25	0.19	0.10	0.06
C_3H_8	0.44	0.49	0.41	0.39
C_4H_8	0.13	0.10	0.06	0.04
C_4H_{10}	0.24	0.26	0.21	0.21
TOF of liquid products (h^{-1})				
CH_3OH	2.90	1.29	0.83	0.42
C_2H_5OH	1.89	1.07	0.65	0.43
CH_3COOH	10.4	6.32	4.24	2.82

[a] H_2 selectivity (%) = [(moles of H_2 produced)/(moles of C in gas phase)] × (2/5) × 100.
[b] Hydrocarbon selectivity (%) = [(moles of C in gaseous alkanes)/(total moles of C in gas products)] × 100.
[c] Below the detection limit.

at conversions below 9%. As proven by our previous work [16], the transport limitations can be excluded under the present reaction conditions. As shown in Table 2, the selectivities to H_2 and hydrocarbons evolve in opposite trends: with the increment of the nominal Co/Zn ratio from 1/3 to 2/1, the selectivity to H_2 decreases from 89% to 52%, while the selectivity to hydrocarbons increases from 29% to 46%. For comparison, on the Raney Ni catalyst and under the same temperature and pressure, the H_2 selectivity is 47%, and the alkane selectivity is 33% at conversion of 13.7% [14], which is even less selective to H_2 than the Co/ZnO-21 catalyst displaying the lowest H_2 selectivity among the Co/ZnO catalysts. In addition, as compared to Raney Ni, the Co/ZnO catalysts produce much less CO in the outlet gas (below the detection limit of ~50 ppm), which is significant especially for fuel cells in which anode materials are vulnerable to CO poisoning [32]. The present work therefore demonstrates the potential of cobalt as an effective component in formulating a CO-free H_2-specific catalyst for APR of ethylene glycol. Also found in Table 2 are small amounts of alkenes (C_2H_4, C_3H_6, and C_4H_8), which are not available on Raney Ni [14]. Such differences are attributable to the fact that Co is an excellent FTS catalyst tending to produce alkenes [19,33].

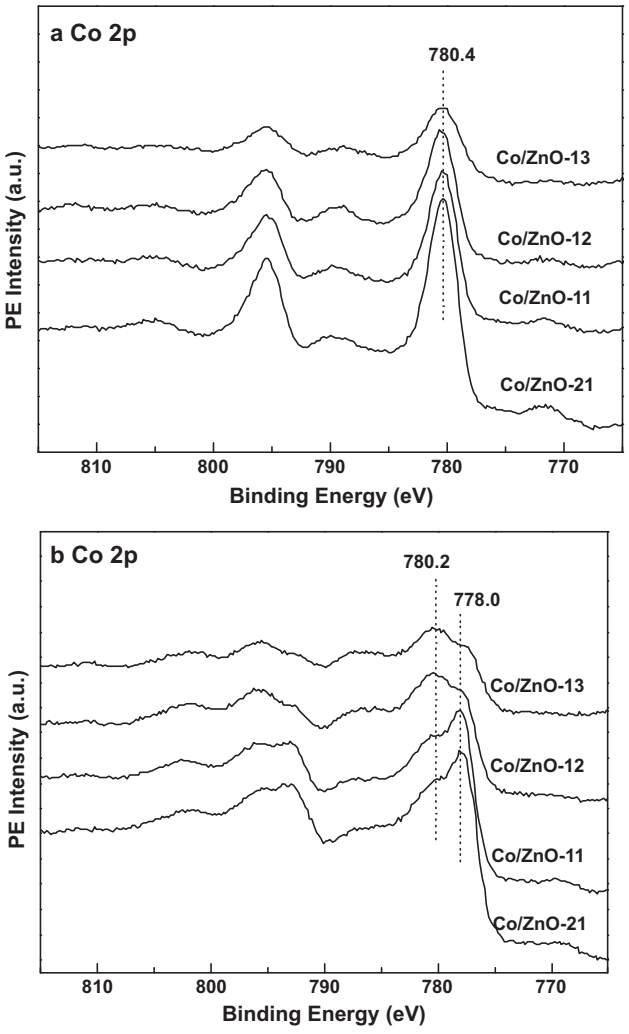

Fig. 5. Co 2p XPS spectra of the Co/ZnO samples (a) before and (b) after reduction.

According to the kinetic data presented in Table 2, when the nominal Co/Zn ratio is increased from 1/3 to 2/1, the turnover frequency (TOF) of H_2 drops greatly from 101.4 to 27.9 h^{-1}, while the TOF of hydrocarbons using CH_4 as a representative only decreases slightly. The concomitant decrement in the TOFs of H_2 and CO_2 with the increment of the Co/Zn ratio strongly implies that the incorporation of ZnO promotes the desirable WGS reaction, which is analogous to the role of ZnO in Cu/ZnO-based WGS catalysts [34,35]. Shishido et al. found that Cu alone showed a weak activity in the WGS reaction, but the binary system formation with ZnO resulted in an obvious enhancement in the activity [34]. Moreover, Rodriguez et al. identified that the Arrhenius activation energy of the WGS reaction decreased from 15.2 kcal mol^{-1} for Cu(1 0 0) to 12.4 kcal mol^{-1} for Cu/ZnO(0 0 0 $\bar{1}$), attributable to a more efficient cleavage of the O–H bond in water at the existence of ZnO [35]. It should be noted that although the Co/ZnO-13 catalyst has higher TOF of H_2 than Raney Ni (66 h^{-1}) and Raney $Ni_{14}Sn$ (84 h^{-1}) [14], the H_2 production rate on the former (37 μmol g_{cat}^{-1} min^{-1}) is much lower than those on Raney Ni (244 μmol g_{cat}^{-1} min^{-1}) and Raney $Ni_{14}Sn$ (236 μmol g_{cat}^{-1} min^{-1}), which can be attributed to the much lower active surface area of the Co/ZnO-13 catalyst. Future catalyst development work should focus on how to prepare Co/ZnO catalysts with higher dispersions.

In the liquid effluent, methanol, ethanol, and acetic acid are detected. We find that the production rates of acetic acid are the highest than those of methanol and ethanol on the Co/ZnO cata-

Table 3
The conversion and product distribution over the Co/ZnO-21 catalyst in APR of 5 wt% methanol, ethanol and ethylene glycol at 498 K, 2.58 MPa, WHSV of 0.09 h^{-1}, and after 8 h on stream.

Feedstock	Ethylene glycol	Methanol	Ethanol
Conversion (%)	50.5	42.0	19.0
Conversion of C to gas (%)	35.5	41.7	0.1
Gas products (mol%)			
H_2	58.7	67.2	99.7
CO	n.d.[a]	n.d.	n.d.
CO_2	29.8	24.1	n.d.
CH_4	8.3	8.2	0.18
C_2H_4	0.07	0	0
C_2H_6	1.2	0.3	0.08
C_3H_6	0.27	0.02	0
C_3H_8	1.1	0.18	0
C_4H_8	0.13	0	0
C_4H_{10}	0.45	0	0
Liquid product (mol%, excluding unreacted feedstock)			
Methanol	14.1	/	0
Ethanol	8.7	0	/
2-Propanol	2.7	0	0
Acetic acid	74.5	0	92.3
Acetaldehyde	0	0	5.4
Acetone	0	0	0.2
Ethyl acetate	0	0	2.1

[a] Below the detection limit.

lysts. The production of acids from alcohols over ZnO-supported metal catalysts is not uncommon. Shabaker et al. found the formation of glycolic acid and acetic acid in APR of ethylene glycol over Pt/ZnO catalysts [10]. Takezawa and Iwasa detected formic acid intermediates in SR of methanol over Pd/ZnO catalysts [36].

To have a better understanding of the APR pathways of ethylene glycol over the Co/ZnO catalysts, APR of 5 wt% of ethylene glycol, acetic acid, methanol, and ethanol are compared over the Co/ZnO-21 catalyst under 498 K, 2.58 MPa, and WHSV of 0.09 h^{-1}. Table 3 shows that APR of ethylene glycol at a relatively lower WHSV generates methanol, ethanol, acetic acid, as well as 2-propanol in the liquid phase. According to Shabaker et al. [14], the formation of methanol from ethylene glycol proceeds through C–H bond scission on metal sites, followed by C–C bond scission and hydrogenation. The overall reaction can be written as:

$$HOCH_2CH_2OH + H_2 \rightarrow 2CH_3OH \quad (1)$$

Ethanol can be produced from ethylene glycol through O–H bond scission on metal sites, followed by C–O bond scission and hydrogenation:

$$HOCH_2CH_2OH + H_2 \rightarrow CH_3CH_2OH + H_2O \quad (2)$$

Another pathway for the formation of ethanol from ethylene glycol, i.e. dehydration on the support followed by hydrogenation on metal sites [5] can be discarded here, because we found no dehydration product in APR of ethylene glycol over bare ZnO under the same APR conditions.

Acetic acid may arise from the scission of the O–H bond in ethylene glycol on metal sites, followed by desorption and rearrangement in the aqueous phase [5]:

$$HOCH_2CH_2OH \rightarrow CH_3COOH + H_2 \quad (3)$$

An alternative pathway leading to acetic acid will be discussed below.

We find that acetic acid remains intact when it is used separately as the feedstock under the above APR conditions. The APR of methanol only leads to gas products (Table 3). In APR of ethanol, acetic acid is identified as the primary liquid product (>90 mol%) (Table 3), suggesting the possibility of the formation of acetic acid through ethanol during APR of ethylene glycol. It should be noted that under the present APR conditions, the main reaction is not the reforming of ethanol, which should otherwise produce both H_2 and CO_2, as ethanol can only be reformed on Co-based catalysts at much higher temperatures [21,23,37,38]. Thus, the formation of acetic acid as the primary product clearly indicates that ethanol mainly undergoes the reaction [39]:

$$C_2H_5OH + H_2O \rightarrow CH_3COOH + 2H_2 \quad (4)$$

On the other hand, acetone, rather than 2-propanol formed in APR of ethylene glycol, is detected in APR of ethanol. It is well documented that acetone can be produced through ethanol via the reaction [39,40]:

$$2C_2H_5OH \rightarrow CH_3COCH_3 + CO + 3H_2 \quad (5)$$

The 2-propanol detected in APR of ethylene glycol may form via the hydrogenation of acetone in the H_2-rich atmosphere because of the better reforming reactivity of ethylene glycol.

Based on these control experiments and literature works, it is evident that besides the reaction pathways of ethylene glycol with water proposed by Cortright et al. [2], there are additional pathways from ethanol to acetic acid and 2-propanol and via the FTS reaction to alkenes in APR of ethylene glycol over the Co/ZnO catalysts.

4. Conclusion

In APR of ethylene glycol, the Co/ZnO catalysts prepared by the coprecipitation method could exhibit higher intrinsic activity and H_2 selectivity than the Raney Ni catalyst. Moreover, the Co/ZnO catalysts produced much less CO, which is especially desirable for fuel cell applications, demonstrating the potential of cobalt as an effective component in formulating a H_2-specific catalyst for APR of ethylene glycol. Future catalyst development work should focus on the preparation of Co/ZnO catalysts with higher dispersions to improve the H_2 productivity, which is underway in our laboratory. As to the reaction pathways, besides those proposed previously, reactions from ethanol to acetic acid and 2-propanol and via the FTS reaction to alkenes should also be taken into account for the Co/ZnO catalysts.

Acknowledgments

This work was supported by the National Basic Research Program of China (2006CB202502), the NSF of China (20673025, J0730419, 20803011), the Program of New Century Excellent Talents in Universities (NCET-08-0126), the Science & Technology Commission of Shanghai Municipality (10JC1401800, 08DZ2270500), and the State Key Laboratory of Catalytic Materials and Reaction Engineering (RIPP, SINOPEC).

References

[1] D. Das, T.N. Veziroglu, Int. J. Hydrogen Energy 26 (2001) 13–28.
[2] R.D. Cortright, R.R. Davda, J.A. Dumesic, Nature 418 (2002) 964–967.
[3] G.W. Huber, J.W. Shabaker, J.A. Dumesic, Science 300 (2003) 2075–2077.
[4] G.W. Huber, J.N. Chheda, C.J. Barrett, J.A. Dumesic, Science 308 (2005) 1446–1450.
[5] R.R. Davda, J.W. Shabaker, G.W. Huber, R.D. Cortright, J.A. Dumesic, Appl. Catal. B: Environ. 56 (2005) 171–186.
[6] R.R. Davda, J.W. Shabaker, G.W. Huber, R.D. Cortright, J.A. Dumesic, Appl. Catal. B: Environ. 43 (2003) 13–26.
[7] J.W. Shabaker, R.R. Davda, G.W. Huber, R.D. Cortright, J.A. Dumesic, J. Catal. 215 (2003) 344–352.
[8] J.W. Shabaker, J.A. Dumesic, Ind. Eng. Chem. Res. 43 (2004) 3105–3112.
[9] R.R. Davda, J.A. Dumesic, Angew. Chem. Int. Ed. 42 (2003) 4068–4071.
[10] J.W. Shabaker, G.W. Huber, R.R. Davda, R.D. Cortright, J.A. Dumesic, Catal. Lett. 88 (2003) 1–8.
[11] X.H. Liu, K. Shen, Y.G. Wang, Y.Q. Wang, Y.L. Guo, Y. Guo, Z.L. Yong, G.Z. Lu, Catal. Commun. 9 (2008) 2316–2318.
[12] O. Skoplyak, M.A. Barteau, J.G. Chen, J. Phys. Chem. B 110 (2006) 1686–1694.
[13] O. Skoplyak, M.A. Barteau, J.G. Chen, Catal. Today 147 (2009) 150–157.
[14] J.W. Shabaker, G.W. Huber, J.A. Dumesic, J. Catal. 222 (2004) 180–191.

[15] J.W. Shabaker, D.A. Simonetti, R.D. Cortright, J.A. Dumesic, J. Catal. 231 (2005) 67–76.
[16] F.Z. Xie, X.W. Chu, H.R. Hu, M.H. Qiao, S.R. Yan, Y.L. Zhu, H.Y. He, K.N. Fan, H.X. Li, B.N. Zong, X.X. Zhang, J. Catal. 241 (2006) 211–220.
[17] X.W. Chu, J. Liu, M.H. Qiao, J.H. Zhuang, K.N. Fan, X.X. Zhang, B.N. Zong, Chinese J. Catal. 30 (2009) 595–600.
[18] L.J. Zhu, P.J. Guo, X.W. Chu, S.R. Yan, M.H. Qiao, K.N. Fan, X.X. Zhang, B.N. Zong, Green Chem. 10 (2008) 1323–1330.
[19] A.Y. Khodakov, W. Chu, P. Fongarland, Chem. Rev. 107 (2007) 1692–1744.
[20] P.R. de la Piscina, N. Homs, Chem. Soc. Rev. 37 (2008) 2459–2467.
[21] J. Llorca, N. Homs, J. Sales, P.R. de la Piscina, J. Catal. 209 (2002) 306–317.
[22] R.C. Reuel, C.H. Bartholomew, J. Catal. 85 (1984) 63–77.
[23] J. Llorca, P.R. de la Piscina, J.A. Dalmon, J. Sales, N. Homs, Appl. Catal. B: Environ. 43 (2003) 355–369.
[24] C. Tang, C. Wang, S. Chien, Thermochim. Acta 473 (2008) 68–73.
[25] Y. Zhang, D. Wei, S. Hammache, J.G. Goodwin, J. Catal. 188 (1999) 281–290.
[26] N.N. Madikizela-Mnqanqeni, N.J. Coville, J. Mol. Catal. A: Chem. 225 (2005) 137–142.
[27] M. Haneda, Y. Kintaichi, N. Bion, H. Hamada, Appl. Catal. B: Environ. 46 (2003) 473–482.
[28] Z. Zsoldos, L. Guczi, J. Phys. Chem. 96 (1992) 9393–9400.
[29] S. Velu, K. Suzuki, C.S. Gopinath, J. Phys. Chem. B 106 (2002) 12737–12746.
[30] Y. Pei, P.J. Guo, M.H. Qiao, H.X. Li, S.Q. Wei, H.Y. He, K.N. Fan, J. Catal. 248 (2007) 303–310.
[31] B. Ernst, S. Libs, P. Chaumette, A. Kiennemann, Appl. Catal. A: Gen. 186 (1999) 145–168.
[32] R.A. Lemons, J. Power Sources 29 (1990) 251–264.
[33] M.A. Vannice, J. Catal. 37 (1975) 449–461.
[34] T. Shishido, M. Yamamoto, D.L. Li, Y. Tian, H. Morioka, M. Honda, T. Sano, K. Takehira, Appl. Catal. A: Gen. 303 (2006) 62–71.
[35] J.A. Rodriguez, P. Liu, J. Hrbek, J. Evans, M. Pérez, Angew. Chem. Int. Ed. 46 (2007) 1329–1332.
[36] N. Takezawa, N. Iwasa, Catal. Today 36 (1997) 45–56.
[37] J. Llorca, J.A. Dalmon, P.R. de la Piscina, N. Homs, Appl. Catal. A: Gen. 243 (2003) 261–269.
[38] C.B. Wang, C.C. Lee, J.L. Bi, J.Y. Siang, J.Y. Liu, C.T. Yeh, Catal. Today 146 (2009) 76–81.
[39] A. Haryanto, S. Fernando, N. Murali, S. Adhikari, Energy Fuels 19 (2005) 2098–2106.
[40] J. Llorca, P.R. de la Piscina, J. Sales, N. Homs, Chem. Commun. (2001) 641–642.